Taylor & Francis
Taylor & Francis Group

Journal of Macromolecular Science, Part A
Pure and Applied Chemistry

ISSN: 1060-1325 (Print) 1520-5738 (Online) Journal homepage: https://www.tandfonline.com/loi/lmsa20

Polyurethane-TiO_2 nanocomposite coatings from sunflower- oil-based amide diol as soft segment

Manawwer Alam, Naser M. Alandis, Fahmina Zafar, Eram Sharmin & Yasser M. Al-Mohammadi

To cite this article: Manawwer Alam, Naser M. Alandis, Fahmina Zafar, Eram Sharmin & Yasser M. Al-Mohammadi (2018) Polyurethane-TiO_2 nanocomposite coatings from sunflower- oil-based amide diol as soft segment, Journal of Macromolecular Science, Part A, 55:10, 698-708, DOI: 10.1080/10601325.2018.1526638

To link to this article: https://doi.org/10.1080/10601325.2018.1526638

Published online: 16 Oct 2018.

JOURNAL OF MACROMOLECULAR SCIENCE, PART A: PURE AND APPLIED CHEMISTRY
2018, VOL. 55, NO. 10, 698–708
https://doi.org/10.1080/10601325.2018.1526638

Polyurethane-TiO_2 nanocomposite coatings from sunflower- oil-based amide diol as soft segment

Manawwer Alam[a], Naser M. Alandis[a], Fahmina Zafar[b], Eram Sharmin[c], and Yasser M. Al-Mohammadi[d]

[a]Department of Chemistry, College of Science, King Saud University, Riyadh, Saudi Arabia; [b]Inorganic Materials Research Laboratory, Department of Chemistry, Jamia Millia Islamia, New Delhi, India; [c]Department of Pharmaceutical Chemistry, College of Pharmacy, Umm Al-Qura University, Makkah Al-Mukarramah, Saudi Arabia; [d]Environmental Science, College of Science, King Saud University, Riyadh, Saudi Arabia

ABSTRACT

Vegetable oil based environmentally friendly polyurethane-TiO_2 nanocomposite coatings have been synthesized by using sunflower oil derived diol, toluene diisocyanate and TiO_2 nanoparticles. The chemical structure was confirmed by FTIR and NMR techniques while physico-chemical testing was carried out by standard laboratory methods. Physico-mechanical and anticorrosive tests of the coatings (in different corrosive media) have been investigated by standard methods. In addition to this the morphology and thermal stability behavior of the coatings have been carefully investigated by different techniques like XRD, TEM, TGA/DTG and DSC. The comparison of the performance of nanocomposites with the respective virgin polyurethane coatings reveals that the dispersion of nanoTiO_2 enhanced the mechanical, corrosion and thermal stability behavior of the polymer. The synthesized nanocomposites can be used safely upto 250–275 °C. These sunflower oil derived polyurethane nanocomposites can be used in the world of protective coatings, as an alternative of petroleum derived corrosion protective coating materials.

ARTICLE HISTORY
Received 16 April 2018
Accepted 14 September 2018

KEYWORDS
Sunflower oil; TiO_2; nanocomposite; coating

1. Introduction

Renewable resources such as seed oils derived polymeric materials for coatings are receiving great attention due to the present economic concerns and environmental hazards. During the last few decades, seed oils have been extensively studied as potential starting materials for bio-renewable polymers because of their ready availability from horticultural resources, green origin, inherent biodegradability, low cost, non-toxicity and versatile applications.[1,2] A number of polymers have been prepared from seed oils via various chemical transformations that include oligomerization, free radical, cationic, metathesis, condensation, addition polymerizations and others.[1–4] The prepared polymeric materials exhibit a wide range of properties that suggest their use as replacement for petroleum based polymeric materials.[2]

Sunflower oil (SfO) is obtained from the seeds of sunflower (*Helianthus annuus*). It is a non-volatile oil having fatty acid composition[5]: palmitic acid-6.3%, stearic acid-4.2, oleic acid-18.3%, linoleic acid-69%, linolenic acid-0.4% and other-18.3%. SfO has been used for the development of different polymers for various fields of applications.[5–8]

Polyurethane (PU) is one of the most versatile polymers that possess a wide range of industrial applications such as tubings, footwear, industrial machinery, elastic fibers, rigid insulators, soft flexible foam, medical devices, paints, coatings and others. Polyurethane PU is composed of hard and soft segments. PU are considered as one of the growing industrial market due to their excellent abrasion resistance, flexibility at low temperature, and excellent chemical, mechanical and physical properties.[9] They are obtained by the reaction of di-polyol(soft segment) and diisocyanate(hard segment) which are petroleum derivatives.[10] Research has been carried out to develop these segments from bio-derived materials.[11–13] Seed oil based di-/poly-ols have been prepared and used for polyurethane synthesis with high bio-contents. Such seed oil derived PU have been used as protective coatings, with comparable coating performance to that of petroleum derived polyurethanes coatings.[2,12,14] It was found that the incorporation of nanoparticles may provide extensive opportunities for enhancement of coating performance such as corrosion resistance and mechanical properties.[15,16] So, many nanoparticles such as ZnO, CuO, SiO_2, clay, CNT, TiO_2 have been incorporated in PU matrix, to modify them for advance coatings applications.[17–23] Nanoparticles of TiO_2 have aroused a great interest for their potential in photo-catalyst, as semiconductors in solar and fuel cells, chemical sensors, catalyst support for oxides and group VIII metals, as construction ceramic in nano filtration membrane, biomedical materials, in antifogging and self-cleaning glass coatings and others because of their peculiar properties and advantages over bulk and micro-sized TiO_2 particles.[17,24,25]

CONTACT Manawwer Alam malamiitd@gmail.com Department of Chemistry, College of Science, King Saud University, P. O. Box 2455, Riyadh 11451, Saudi Arabia.
Color versions of one or more of the figures in the article can be found online at www.tandfonline.com/lmsa.

This manuscript reports the incorporation of TiO_2 into polyurethane derived from sunflower oil based amide diol, which to the best of our knowledge has not been reported yet.[15,26] To that end, synthesis of polyurethane and preparation of TiO_2 containing nanocomposite was also considered in the present work. The prepared materials were characterized and the physico-mechanical and corrosion inhibition of virgin and modified coatings were investigated.

2. Experimental

2.1. Materials

Sunflower oil [SfO] (Haley, Abu Dhabi Vegetable oil Co. L.L.C. Abu Dhabi, UAE), diethanol amine (Winlab, UK), sodium metal (BDH Chemical Ltd. Poole, England), methanol (Sigma Aldrich, Louis, USA), toluene 2,4-diisocyanate (Acros Organics, USA), Titanium isopropoxide (Aldrich Chemical, UK), and xylene (Winlab, UK) were of analytical grade. TiO_2 has been prepared by our previously reported method.[26]

2.2. Synthesis of sunflower oil based amide diol (HESfA)

HESfA has been synthesized as per our previously reported method with some modification.[27] Diethanolamine (50 g), SfO (60 g) and freshly prepared sodium methoxide (0.26 g) were taken in three necked flask that was connected to a dropping funnel and thermometer. The flask containing all reagents was placed on magnetic stirrer and heated at 120 ± 5 °C with continuous stirring. Thin layer chromatography (TLC) was used to monitor the progress of reaction. After completion of reaction, the heating was turned off and the material was cooled down to room temperature. Now, the material was dissolved in diethyl ether and wash with aqueous solution of NaCl (15%) by using separating funnel, finally dried over anhydrous Na_2SO_4. The ethereal layer was taken off and the ether was removed by using vacuum evaporator. Finally, light brown viscous HESfA was obtained (Yield: 86%).

2.3. Synthesis of poly (urethane–sunflower fattyamide)/ TiO_2 nanocomposite[PUSfFANC)

TiO_2 (methanolic solution, sonicated at room temperature), 1-3wt% (with respect to HESfA) was taken as a modifier. HESfA and TDI (1:1 ratio, w/w) were used for the synthesis of **PUSfFANC**. 1 mmol of HESfA was taken in three necked flask and to this was added alcoholic TiO_2 solution and sonicated for 30 min. Then the flask was placed on magnetic stirrer and a dropping funnel, thermometer and condenser were connected to it. Now, the contents were heated at 80 ± 5 °C with continuous stirring. After completion of reaction, that was confirmed by the appearance of clear solution. TDI (1mmol) solution (prepared with 8–10% DMF) was added then stirring the contents were again heated for further 30 min at 120 ± 5 °C. TLC and FTIR were used to monitor the progress of the reaction. The synthesized systems were abbreviated as PUSfFANC-1, PUSfFANC-2 and PUSfFANC-3 (last numeral implied wt % of TiO_2).Virgin poly(urethane-sunflower fattyamide) (PUSfFA) was synthesized by using aforementioned method except the step of nanoTiO_2 addition.

2.4. Preparation of coatings

40 wt % solution of PUSfFNA and all the compositions of PUSfFANC was prepared and applied on the metal strips by using brush techniques. The coated metal strips were kept undisturbed for drying at ambient temperature.

3. Characterization techniques

3.1. Thin layer chromatography (TLC)

Standard laboratory method was used to check the progress of reactions.

3.2. Physico-chemical tests

Specific gravity (ASTM D 1475), Acid value (ASTMD555-61), Hydroxyl value ((ASTMD1957-86), Iodine value (ASTM D5556) Refractive index (Abbe refractometer, ModelR-4 Indian Rajdhani Scientific Instrument Co. India).

3.3. Spectral analysis

FTIR spectrophotometer, Prestige-21, FTIR-8400S, Shimadzu Corporation, Kyoto, Japan, with NaCl cell.^{1}H and ^{13}C NMR, JeolDPX400MHz (Japan) using deuterated chloroform as solvent and tetramethylsilane as internal standard.

3.4. Thermal analysis

TGA/DSC (Mettler Toledo AG, Analytical CH8603 Schwerzenbach, Switzerland) heating rate 10 °C/min in N_2 atmosphere.

3.5. Coating thickness

Thickness gauge (Model 456, Elcometer Instrument, Manchester, UK).

3.6. Physico-mechanical tests

Scratch hardness (BS 3900), pencil hardness test (ASTM D3363)(Wolf-Wilborne tester, Sheen instrument, England), impact resistance (IS; 101 part 5/sec-3, 1998), bend test (ASTM D3281-84), cross hatch adhesion test (ASTM D3359-02).

3.7. Morphology

XRD, SEM (JEOL, JSM 7600F, Japan), TEM (JEM2100F, Jeol, Japan)

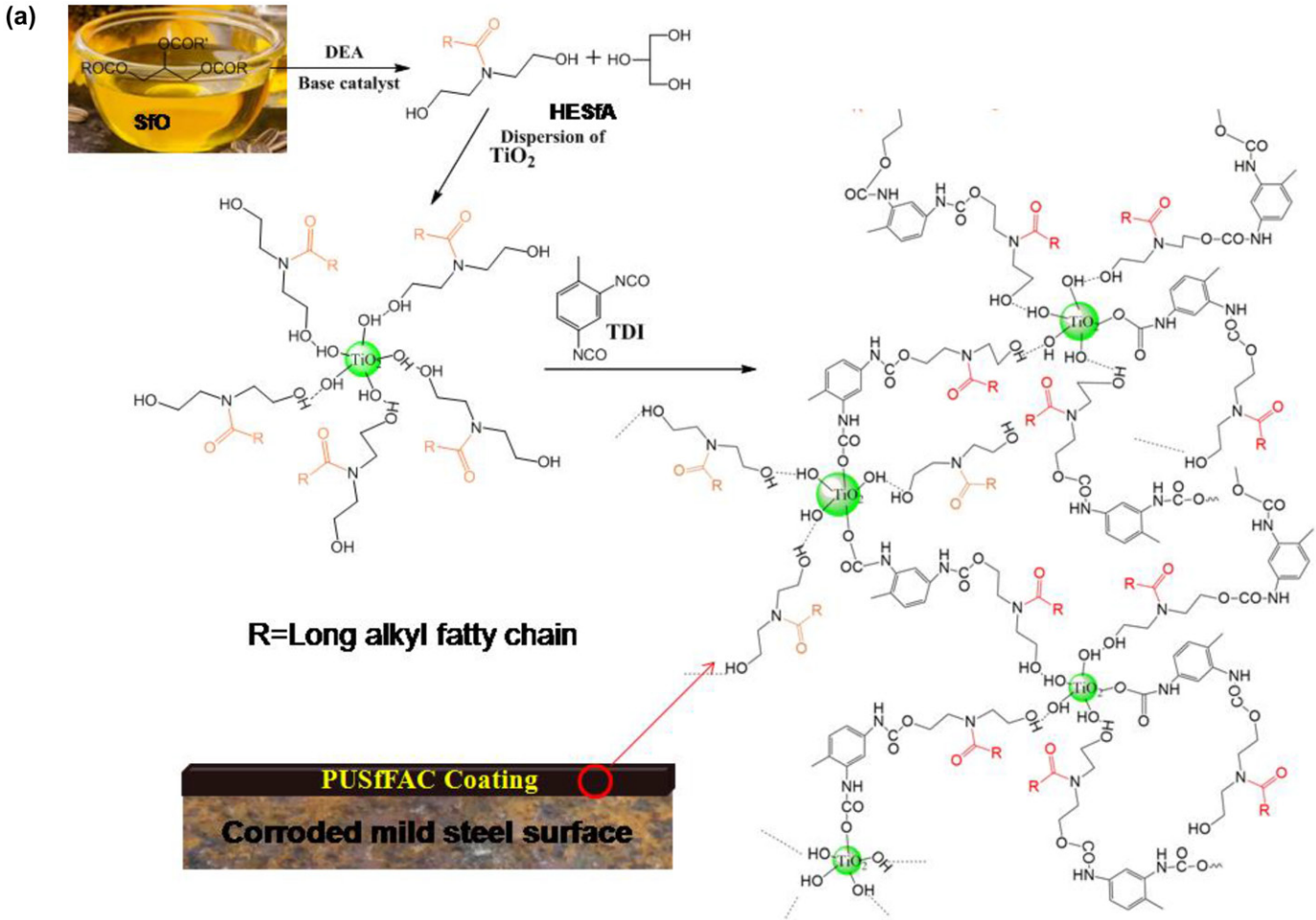

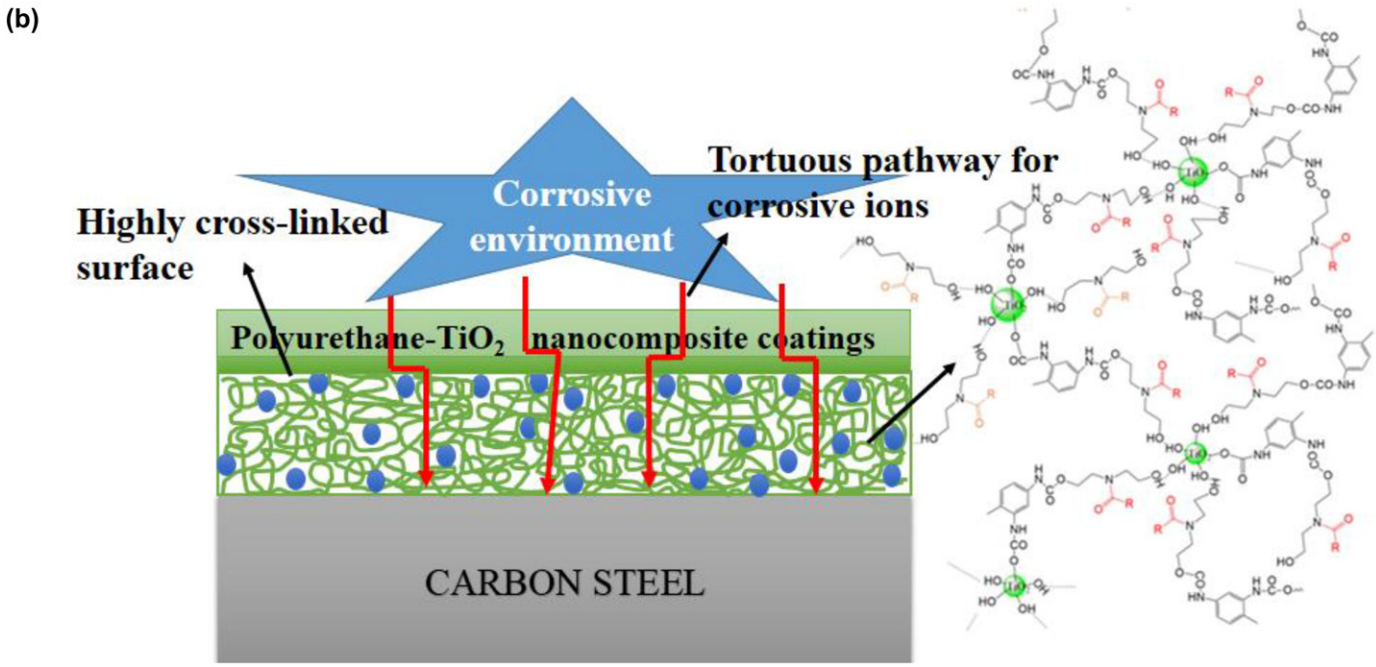

Scheme 1. a. Synthesis of PUSfFANC. b. Schematic representation of corrosion inhibition of carbon steel by through PUSfFANC coating.

Corrosion resistance performance of all the compositions of **PUSfFANC** and virgin **PUSfFA** were performed by Potentiodynamic polarization measurements at room temperature in different corrosive environments: 3.5 wt % HCl, 5 wt% NaCl and tap water (163.303, 139.375 and 35.320 ppm respectively for Cl^{-}, S^{2-} and Ca^{2+} ions

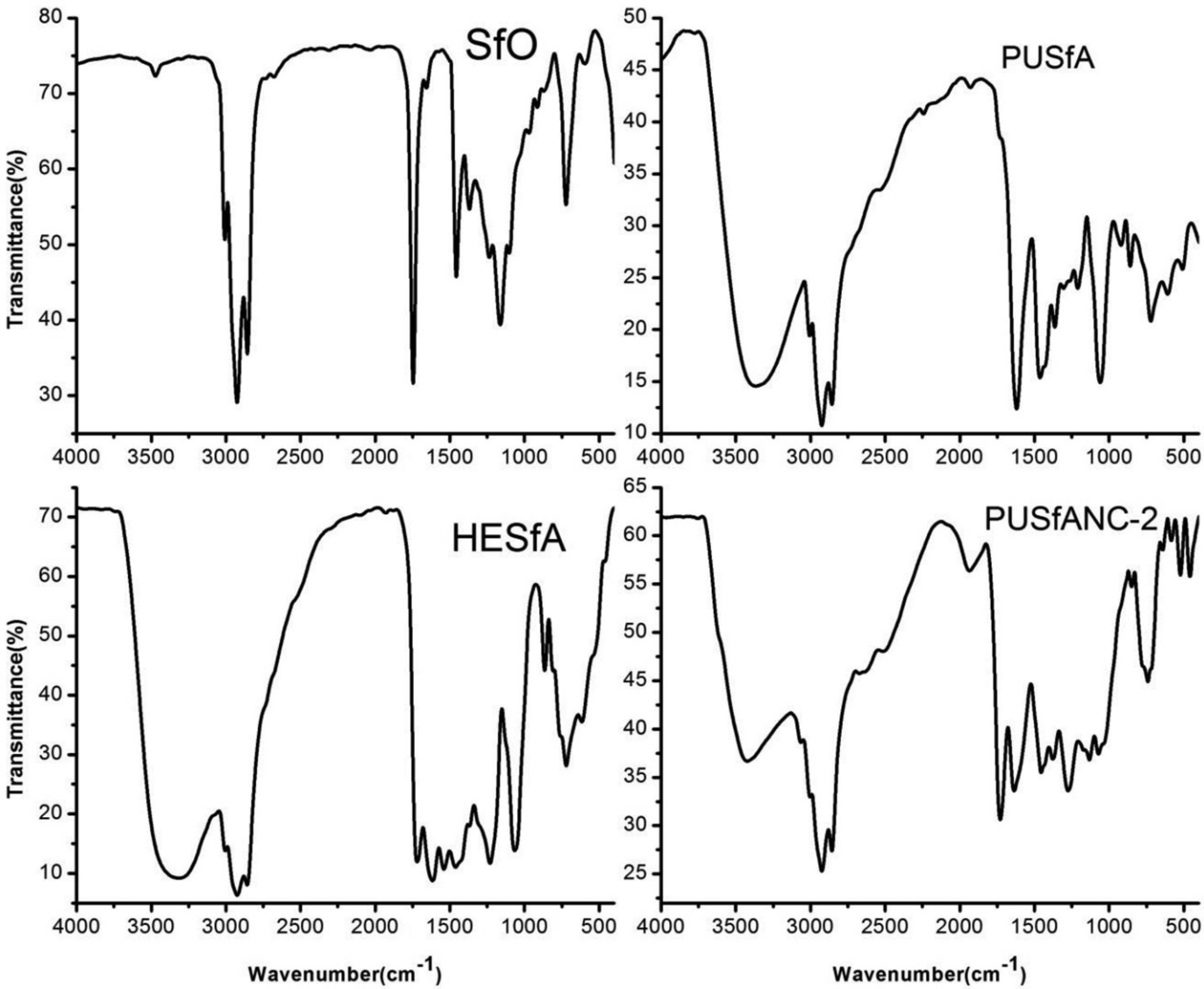

Figure 1. FTIR spectra of SfO, HESfA, PUSfFA and PUSfFANC-2.

measured by ICP Mass). It was performed in three different electrode, (1) a platinum electrode as counter electrode, (2) saturated calomel electrode as reference electrode and, (3) specimen(coated and uncoated mild steel strips) as working electrode. The exposed surfaces area of working electrode that was embedded by polytetrafluoroethylene was 1.0 cm^2. The PDP or tafel curves (computer controlled Auto ACDSP with Boukamp software, ACM instrument) were obtained using a sweep rate of 1 mV/s, in the potential range of ±250 mV, with respect to initial open circuit potential.

4. Results and discussion

The reactions involved in the synthesis of PUSfFA and PUSfFANC are given in Scheme. Scheme 1a implies that the reaction is carried out by the reaction of hydroxyl groups of HESfA (that was obtained by the amidation reaction of SfO with base catalyst) and isocyanate group of TDI via addition polymerization reaction without any catalyst. The 1:1 ratio of SfFA and TDI are selected for the present work since the literature reveals that this ratio gives better results for coating applications.[10,27] The reactions carried out in the same pot as "one-pot, two-step reaction". The first step involved the dispersion of nanoTiO_2 (1, 2 and 3 wt %) in HESfA. It was carried out by sonication followed by heating the same at 80 ± 5 °C with continuous stirring. The second step (in the same pot) involves the addition polymerization reaction between hydroxyl and isocyanate groups at 120 ± 5 °C resulting into PUSfFANC. PUSfFA and all the compositions of PUSfFANC are completely soluble in THF, ether, xylene, CCl_4, $CHCl_3$, DMSO and DMF and partially soluble in lower alcohols whereas insoluble in water. The long alkyl chain and polar groups can be considered responsible for the solubility of PUSfFA and all the composition of PUSfFANC.

4.1. FTIR analysis

Figure 1 shows the FTIR spectra of SfO, HESfA, PUSfFA and PUSfFANC-2. FTIR spectrum (Figure 1a) of SfO shows the characteristic peaks of triglyceride at 1745.77 cm^{-1}

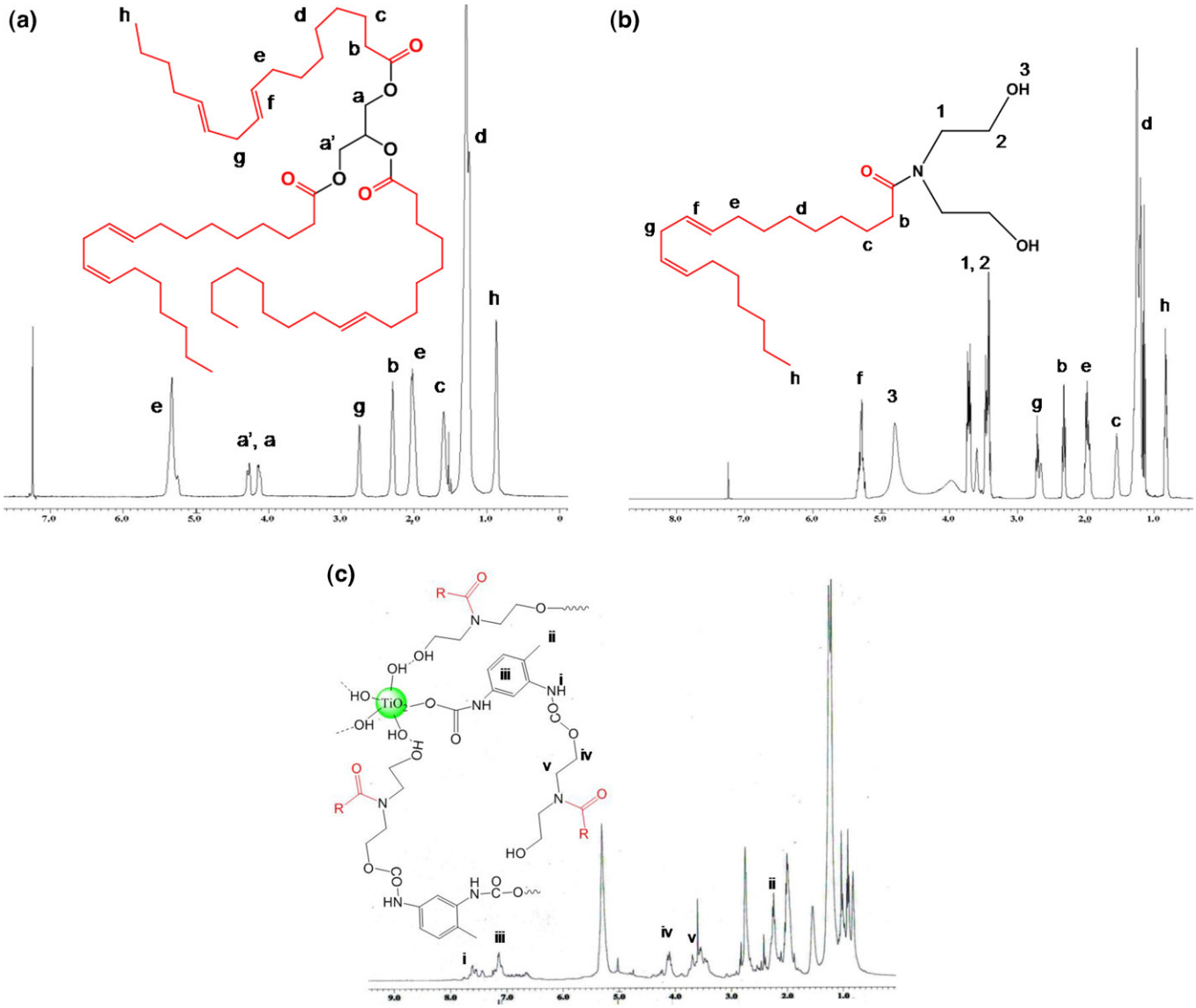

Figure 2. a. ^{1}H NMR spectra of SfO. b. ^{1}H NMR spectra of HESfA. c. ^{1}H NMR spectra of PUSfFA.

(>C=O ester, str.), 1237.98 cm^{-1}, 1163.13 cm^{-1} and 1099.24 cm^{-1} (C-O asym str. of ester), 3008.70 cm^{-1} (=C-H str. Olefin), 2925.89 $cm^{-1}$and 2854.74 cm^{-1}(CH_2 str. asym and symm) along with 1461.71 cm^{-1} and 1377.67, 722.28 cm^{-1} (CH_2sym and CH_3sym bending), 722.28 cm^{-1} [=C-H deformation (cis) and methylene rocking]. The spectrum (Figure 1b) of HESfA shows the appearance of all the characteristic peaks of alkyl fatty chain along with additional peaks at 3349.20 cm^{-1}, 1622.45 cm^{-1}, 1430–1417 cm^{-1} and 1060.31 cm^{-1}, correlated to O-H str, carbonyl [>**N-C**(=O)- amide carbonyl], C-N str [>**N-C**(=O)- amide carbonyl], C-OH str. (primary alcohol), respectively. The characteristic peaks of ester triglyceride of SfO completely disappear in FTIR spectrum of HESfA, while absorption bands typical for hydroxyl groups appear distinctively, supporting the amidation reaction at the given functional group, resulting in the formation of diol with amide linkage, by the amidation of SfO with DEA in presence of base catalyst.

The presence of characteristic bands of urethanes linkages in the spectrum (Figure 1c) of PUSfFA are observed at 1711.24 cm^{-1}, 1229.80 cm^{-1}, 698 cm^{-1}, 1069.43 cm^{-1} and 1537.47cm^{-1} for > C=O str., NCOO-str., N-H, -O-C=O and C-N str./N-H out-of- plane bending of urethane groups, respectively. Moreover, the spectrum shows peaks at 3015.07 $cm^{-1}$and 725.00 cm^{-1}, which are due to ArC=C and Ar-ring bending along with the bands of long alkyl chain. In addition to this, the broad peak centered at 3312.19 cm^{-1} also observed in the spectrum of PUSfFA can be attributed to the stretching vibration of urethane N-H and alcoholic O-H overlapped with each other. These observations can be correlated to the addition polymerization reaction of –NCO group of TDI with –OH groups of HESfA. The broadening of peaks is also observed in the spectrum due to the hydrogen bonding. The spectrum (Figure 1d) of PUSfFANC-2 shows the characteristic peaks of urethane groups as observed in PUSfFA along with the presence of additional peak at 461.20 cm^{-1} in the spectrum, assigned to O-Ti-O[16]. Moreover, the blue shift is also observed in the range of carbonyl (observed at 1732.68 cm^{-1} and 1275.25 cm^{-1} instead of 1711.24 cm^{-1} and 1229.80 cm^{-1}) and N-H

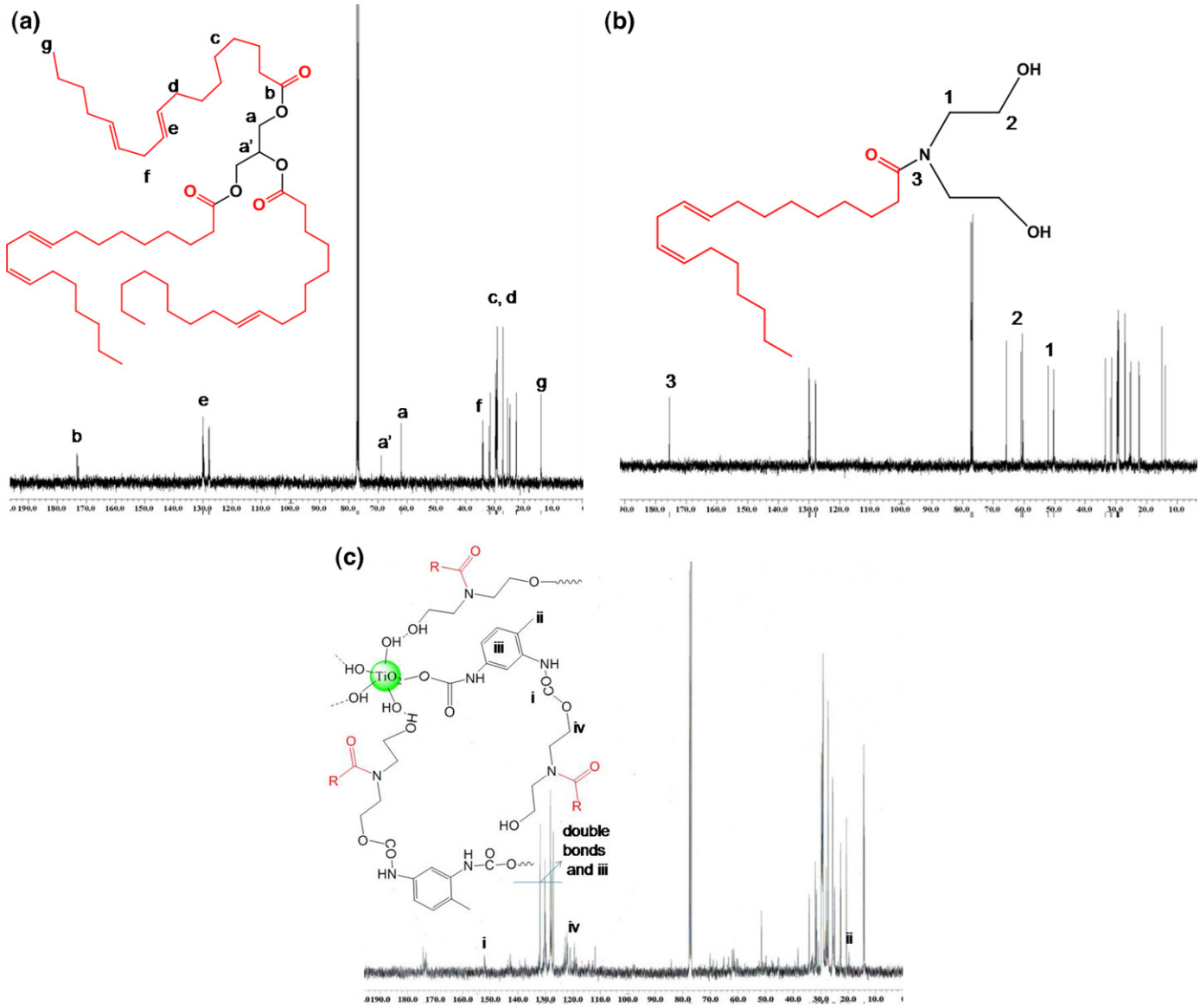

Figure 3. a. ^{13}C NMR spectra of SfO. b. ^{13}C NMR spectra of HESfA. c. 13C NMR spectra of PUSfFA.

(observed at 3418.81 cm^{-1} instead of 3312.19) of urethane that is correlated to the electron induced effect taking place due to TiO_2 dispersion. The absence of free –NCO peaks in both the spectra of PUSfFA and PUSfFANC-2 supports the complete reaction of NCO with –OH.

4.2. NMR analysis

The structure of the material was confirmed by comparing the NMR spectra of SfO, HESfA, and PUSfFANC (Figures 2a–c and 3a–c). SfO spectrum shows the following NMR peaks at **^{1}H-NMR** (Figure 2a) ($CDCl_3$/TMS, δ, ppm) at 5.32 (–C **H**=CH–, f), 4.1–4.27 (–C **H**$_2$/C **H**–OCO, a), 2.75 (=HC-C **H**$_2$-CH=, g), 2.29 (–OCC**H**$_2$, b), 2.02 (–C **H**$_2$–CH = CH–, e),1.59 (–OCCH$_2$C **H**$_2$, c), 1.23–1.28 (–C **H**$_2$–, fatty acid chain, d), 0.87 (–C **H**$_3$, h). **^{13}C-NMR** (Figure 3a) ($CDCl_3$/TMS, δ, ppm) peak at 172.00–172.50 (–O **C**=O, ester carbonyl, b), 130.00–127.88 (–H **C**= **C**H–; olefin carbon, e), 62.09, 69.5 (– **C**H/ **C**H$_2$–OCO, a, a′), 34.5 (=HC- **C**H$_2$-CH=, f), 29.69-29.11 (CH$_2$ fatty acid chain, c), 27.18 (**C**H$_2$–C=C–, d) and 14 (– **C**H$_3$, g). The spectrum of FASfO (Figure 2b) shows **^{1}H-NMR ($CDCl_3$/TMS, δ, ppm)** peaks at 5.32–5.28 (–C **H**=C **H**–), 4.80 (–O **H**), 3.73 and 3.70 (t, –C **H**$_2$–N<), 3.47–3.42 (–C **H**$_2$–OH), 2.33 (–C **H**$_2$– C(=O)–N<}, 2.00 (–C **H**$_2$–CH = CH–), 1.55 (m, –OCC **H**$_2$ CH$_2$), 1.26-1.20 (–C **H**$_2$–, fatty acid chain), 0.84 (–CH$_3$). **^{13}C-NMR** (Figure 3b) **($CDCl_3$/TMS, δ, ppm)** peaks at 175.53 (– **C**(=O)–N–, amide carbonyl), 130.12–127.9 (–H **C**= **C**H–; olefin carbon), 60.30–65.77 (**C**H$_2$–OH), 50.35–52.10 (**C**H$_2$–N), 29.56–22.2 (– **C**H$_2$), 27.12 (**C**H$_2$–C=C–), 14.02(–**C**H$_3$).

PUSfFANC-2 (Figure 2c) shows ^{1}H-NMR ($CDCl_3$/TMS, δ, ppm) peaks at 5.32–5.28 (–C **H**=C **H**–), 5.02 (low intensity, -O **H**)], 4.13–4.09 [C **H**$_2$-OC(=O)NH–, urethane)], 3.59–3.54

Table 1. Physico-chemical analysis of SfO, HESfA, PUSfFA and PUSfFA NC nanocomposite.

Properties/code	SfO	HESfA	PUSfFA	PUSfFANC-1	PUSfFANC-2	PUSfFANC-3
Specific gravity	0.9205	0.92	0.930	0.931	0.932	0.932
Refractive index	1.4710	1.472	1.478	1.4805	1.4808	1.4810
Hydroxyl value (%)	0.80	6.4	4.5	4.0	3.8	3.4
Iodine value	126	62	42	43	44	45

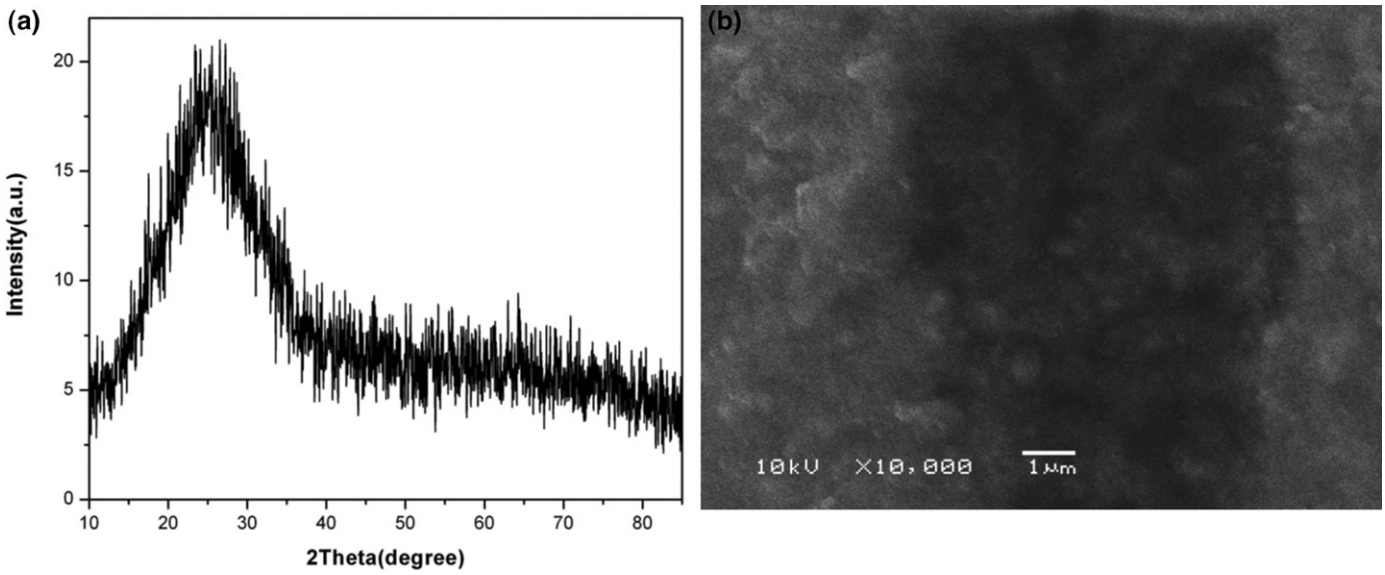

Figure 4. a. XRD graph of PUSfFANC-2 nanocomposite. b. SEM image of PUSfFANC-2 nanocomposite.

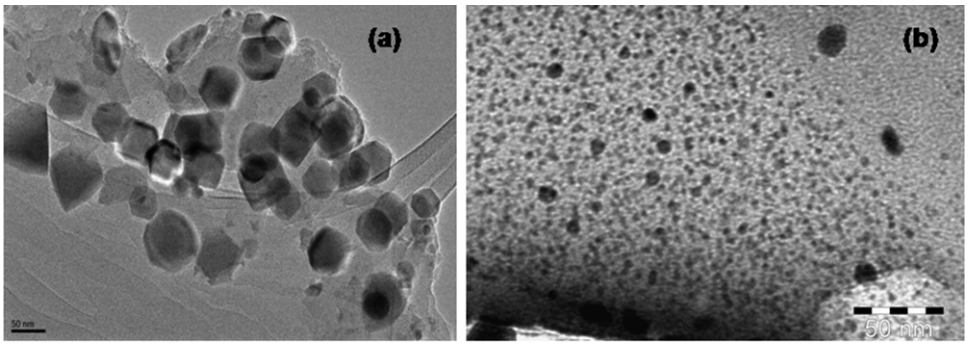

Figure 5. a. TEM image of TiO_2 nanoparticle. b. TEM image of PUSfFANC-3 naocomposite.

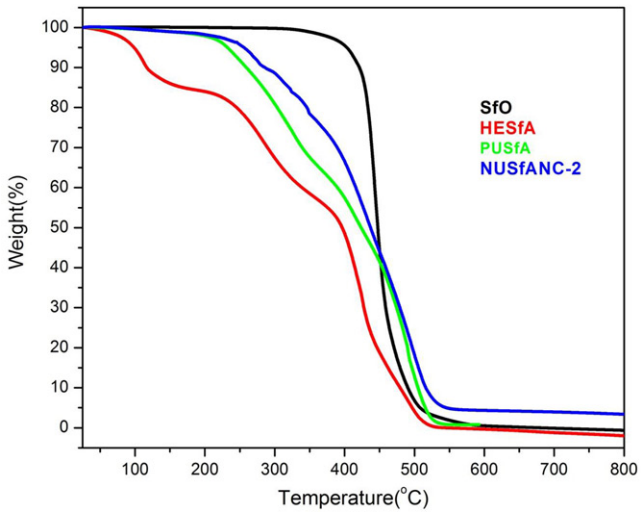

Figure 6. TGA thermogram of SfO, HESfA, PUSfFA and PUSfFANC.

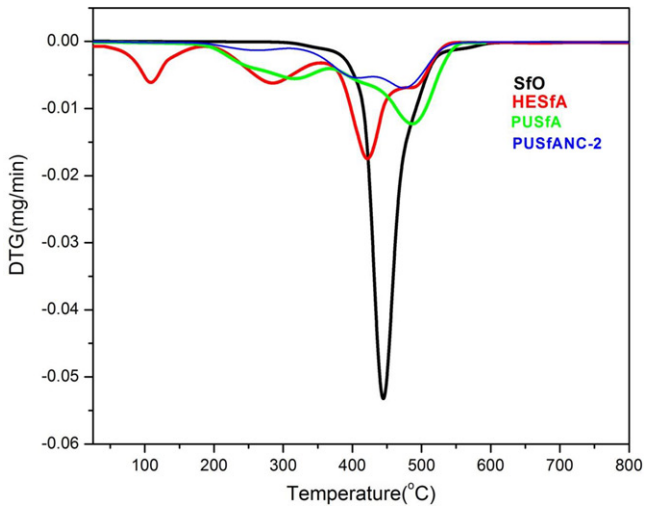

Figure 7. DTG thermogram of SfO, HESfA, PUSfFA and PUSfFANC.

(–C $\underline{H}_2$–N), 2.40 (–C $\underline{H}_2$(C=O)N<}, 2.25 (–C $\underline{H}_3$ of TDI), 2.02 (– $\underline{C}H_2$–CH = CH–), 1.56 (–OCC $\underline{H}_2$-CH_2), 1.31 (–C $\underline{H}_2$–, fatty acid chain), 0.82 (- $\underline{C}H_3$). ^{13}C-NMR (Figure 3c) ($CDCl_3$/TMS, δ, ppm) peaks at 173.28–174.36 ($\underline{C}$=O amide), 152.16 ($\underline{C}$=O urethane and free –NCO), 130.10, 126.00 (–H $\underline{C}$= $\underline{C}$H–, olefin carbon), 127.14–131.94 (Aromatic ring carbons), 62.13–69.00 (–C $\underline{H}_2$–O), 71.4, 59.376 (residual, C $\underline{H}$–OH and C $\underline{H}_2$– OH), 49.77–51.47 (C $\underline{H}_2$–N), 29.74–25.65 (chain C $\underline{H}_2$), 18.50 (C $\underline{H}_3$ attached to aromatic ring), 14.34–14.18 (–C $\underline{H}_3$). These results can further confirm the formation of urethane linkages along with the dispersion of nanoTiO_2.

4.3. Physico-chemical analysis

Physico-chemical tests such as specific gravity, refractive index, hydroxyl value and iodine value are tabulated in Table 1. HESfA is showing higher% of hydroxyl values than that of SfO, which relates to the conversion of triglyceride of SfO to SfFA via amidation. The% hydroxyl value is further decreased with the reaction of TDI that correlated to the consumption of hydroxyl groups by isocyanate groups to form urethane linkages. From PUSfFANC-1 to PUSfFANC-3, the % of hydroxyl value is slightly decreased. The specific gravity, refractive index and iodine values are considerably decreased from SfO to SfFA and PUSfFA, thereafter slightly increased with increased % of TiO_2. These results can be correlated to the formation of PUSfFA from SfO then with nanoTiO_2 (PUSfFANC-1 to PUSfFANC-3) crosslink with TiO_2 structure would be formed. The crosslinking would be due to the electrostatic interactions between surface hydroxyls of nanoTiO_2 with the urethane groups and hydroxyl groups.

4.4. Morphology

Figure 4a depicts the XRD pattern of PUSfFANC-2 that shows the diffraction peak (broad) at $2\theta = 24.2°$. The broadening of the peak can be correlated to the strong interfacial interactions between nanoTiO_2 particles and PUSfFA. The result indicated the amorphous behavior of the nanocomposite. SEM image was taken to investigate the surface morphology of the synthesized PUSfFANC-2 coating (Figure 4b). The image reveals the uniform surface of the coating without any visible cracks and damage with uniform distribution of nanoTiO_2particles, embedded in the polymer matrix. The uniform distribution can be related to the direct attachment of nano TiO_2 particles with the polymer chains that will certainly help to improve the mechanical and corrosion protection performance of the nanocomposite coatings. The uniform or homogenous dispersion of nanoparticles in the polymer matrix is the one condition needed for a nanocomposite to display good mechanical strength reinforcement since in homogeneities may lead to structural defects in the nanocomposite materials.

The particle size and the shape of the nanoparticle of neat TiO_2 and the dispersed particles within the polymer matrix were characterized by TEM analysis. Figure 5a and b show TEM images of nanoTiO_2 and PUSfFANC-2. Figure 5a reveals hexagonal shape of the neat TiO_2 particles with well-defined boundaries and size in the range of 20–50 nm. Figure 5b reveals the uniform dispersion of nanoTiO_2 within polyurethane matrix.

4.5. Thermal analysis

The thermal behavior of SfO, HESfA, PUSfFA and PUSfFANC was carried out by TGA/DTG and shown in Figures 6 and 7. TGA/DTG curves of SfO has showed mainly one step degradation that started from 340 to 550 °C with no residue at 800 °C that is correlated to the decomposition of unsaturated and saturated fatty acids. The TGA/DTG curve of HESfA has showed multistep degradation, which implies that the stability decreases by amidation. But the thermal stability was considerably improved by the polymerization that is urethanation of HESfA with TDI to form PUSfFA and PUSfFANC. The thermal degradation and stability of seed oil based polyurethanes mainly depends on the hard segment and soft segments and their degradation is generally carried out in either 2 or 3 steps process. The first stage is related to hard segment decomposition and evaporation of compounds that are formed. The decomposed compounds are isocyanate and alcohol, primary or secondary amine and olefine, and CO_2. The last steps are related to the decomposition and evaporation of soft segments.

In the spectra of PUSfFA and PUSfFANC, initial very slight weight loss is correlated to the entrapped solvent and moisture. The spectra of both polyurethanes have mainly three step of degradation. The first degradation step occurred in the temperature range of 200–340 °C, second degradation step in the temperature range of 340–450 °C and last degradation step in the temperature range of 450–540 °C.The first step of degradation arises due to the decomposition of labile urethane bonds. The second step can be due to the soft segment chain scission. The last step can be correlated to the decomposition of unsaturated and saturated fatty acids. The thermal stability of PUSfFANC is slightly higher than that of PUSfFA due to the inclusion of TiO_2 nanoparticles.

DSC thermogram (Figure 8) of SfO shows two small endothermic peaks at −26 °C and 57 °C. These peaks are shifted in the case of HESfA at −4 °C and 78 °C. While DSC thermogram (Figure 9) of PUSfANC-2 also shows mainly two endotherms at 69–113 °C centered at 88 °C (first) and 113–225 °C (second broad endotherm) along with very small endothermic peak at 49 °C.These results show a relationship with TGA themogram that the onset of degradation is observed beyond these respective temperatures and

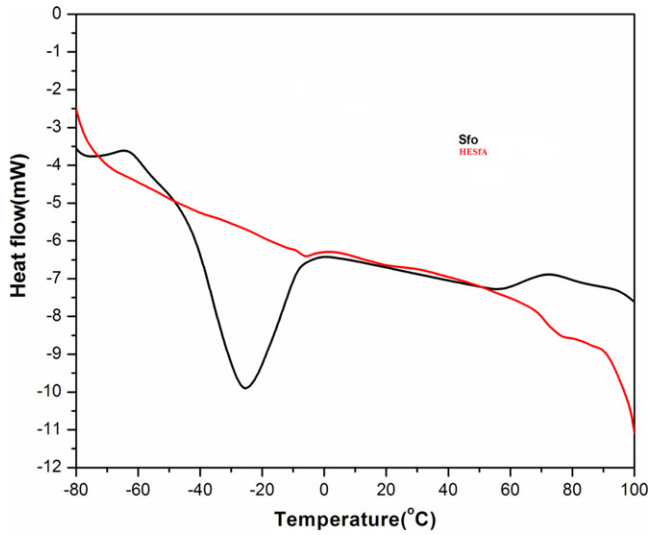

Figure 8. DSC thermogram of of SfO and HESfA.

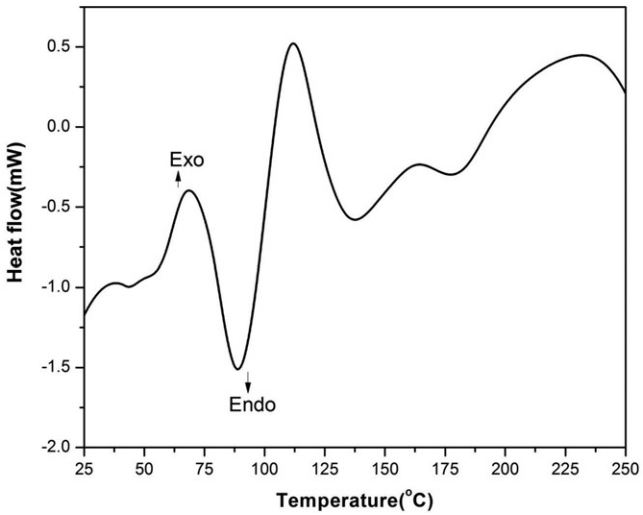

Figure 9. DSC thermogram of of PUSfFANC-2.

Table 2. Physico-mechanical analysis of PUSfFA and PUSfFANC nanocomposite.

Properties/code	PUSfFA	PUSfFANC-1	PUSfFANC-2	PUSfFANC-3
Dry-to- touch (min)	30	25	20	15
Scratch Hardness (kg)	1.0	1.9	2.4	2.3
Cross cut adhesion (%)	95	100	100	100
Impact Resistance (lb/inch)	150 pass	150 pass	150 pass	150 pass
Pencil hardness	1H	2H	3H	2H
Bend test (1/8 inch)	pass	pass	pass	pass
Gloss at 45°	82	84	84	86

these endotherms can be related to the phenomenon of melting points and molecular rearrangements.

4.6. Physico-mechanical behavior

The effect of incorporation of nanoTiO_2 on the mechanical performance such as scratch hardness (kg), pencil hardness, impact resistance (1/8 inch), bend test (lb/inch), cross-hatch adhesion (%) along with gloss (45°) of the nanocomposite coatings was evaluated and compared with PUSfFA coatings. The coatings of PUSfFA and PUSfFANC were prepared on mild steel strip to evaluate the mechanical performance. These coatings were prepared at ambient temperature. The drying time (dry-to-touch) of PUSfFA coatings was found to be 30 minutes whereas in PUSfFANC found to be 25–15 minutes, i.e. the drying time decreases with the inclusion of nano TiO_2. The coatings were left undisturbed to for further 5–6 days to get completely cross-linked (dry-to-hard). The thickness of the films was found to be $95 \pm 5\ \mu$m.

The curing involves a physical process in which solvent evaporation leads to chain entanglement and the chemical process such as primary and secondary reaction of urethane, and autoxidation of double bonds of long alkyl chain leading to cross-linked surface.[18,28,29] The latter process is very slow, that is why the mechanical performance was tested after 5–6 days. The physico-mechanical test results of these coatings are shown in Table 2. The table reveals that the scratch hardness and pencil hardness of the nanocomposite coating increase with TiO_2 up to 2 wt %, and thereafter decrease. The cross-hatch adhesion of PUSfFANC coatings

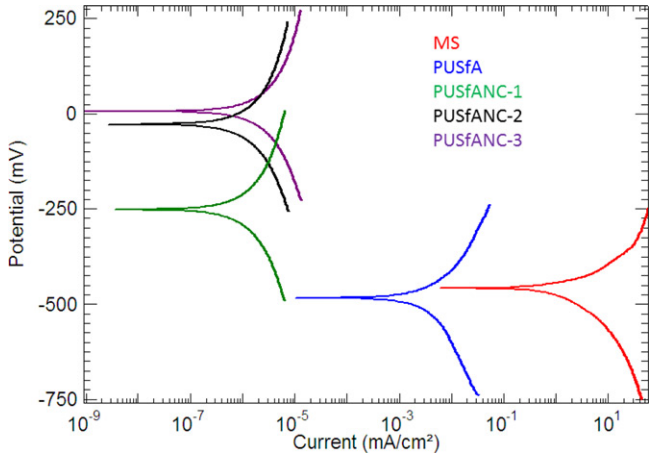

Figure 10. Tafel plot of bare MS, PUSfFA, PUSfFANC-2, PUSfFANC-2 and PUSfFANC-3 in HCl solution.

is higher than PUSfFA coating. The gloss value slightly increases with the inclusion of nanoTiO_2.The coatings of all the systems passed impact resistance test. The presence of nanoTiO_2 increases the adhesion to the surface, hardness along with cross-linking while the long alkyl chains impart flexibility to the nanocomposite coatings. The system PUSfFANC-2 shows the best coating performance amongst them.

4.7. Anticorrosive test

Figure 10 shows the Tafel polarization curve of bare MS, PUSfFA, PUSfFANC-1, PUSfFANC-2 and PUSfFANC-3 after 300 h immersion in 3.5wt% HCl solution. The corrosion potential (E*corr*) of bare MS shifts to more noble values from −459.41 to −5.39 mV with bare MS to PUSfFANC-3 vs. calomel reference electrode. The presence of TiO_2 nanoparticles in PUSfA polarizes the E*corr* in the same direction. As shown in Table 3, Figure 11 shows the polarization curve in 5% NaCl after 300 h immersion; the corrosion potential as well as corrosion current density decrease from bare MS to PUSfFANC-3 (Table 3). Figure 12 indicates the polarization curve in tap water after 300h immersion. I*corr* of bare MS was 1.155E-02 mA/cm^2 and E*corr*-719.55 mV. As compared to PUSfFA, PUSfFANC-1,PUSfFANC-2and PUSfFANC-3 has smaller I*corr* value, 9.898E-08, which nanoparticle containing PUSfANC-3 has better protection than PUSfA.PUSfANC-3 shows higher resistance against the corrosive ions in various media.

These results indicate that TiO_2 nanoparticle containing PUSfA coating acts as a protective barrier on mild steel to enhance the anticorrosion performance. The PUSfANC-3 bio-nanocomposite coatings fashioned compact, uniform, impermeable and hydrophobic nature. An anticorrosive mechanism of nanocomposite coatings can be explained on the basis of the formation of compact, uniform and impermeable barrier coating at the interface of corrosive media and the metal substrate along with presence of nanoTiO2 nanoparticles in organic polymer matrix that prohibit the permeation of corrosive ions through the coating to metal surface (Scheme 1b). The polar functionality (enhances the

Table 3. Tafel analysis parameters of PUSfFANC composite coated and bare mild steel in different corrosive media.

Code	Medium	Ecorr (mV)	Icorr (mA/cm^2)	Ba (mV)	Bc (mV)	CR (mm/yr)	Rp (Ohm.cm^2)
MS	3.5% HCl	−459.41	2.016	40.26	79.09	25.367	6.554
PUSfFA	3.5% HCl	−482.56	2.532E-03	77.98	106.41	2.934E-02	7.728E + 03
PUSfFAC -1	3.5% HCl	−253.28	6.432E-07	121.11	115.44	7.455E-06	3.995E + 07
PUSfFAC -2	3.5% HCl	−25.96	7.335E-07	113.27	120.00	8.501E-06	3.454E + 07
PUSfFAC -3	3.5% HCl	−5.39	1.248E-06	116.71	109.31	1.447E-05	1.966E + 07
MS	5.0% NaCl	−744.81	18.70E-02	69.51	226.26	1.167	123.66
PUSfFA	5.0% NaCl	−659.20	76.94E-04	90.33	224.75	8.891E-02	3.641E + 03
PUSfFAC -1	5.0% NaCl	−534.49	77.43E-08	161.20	177.09	8.974E-06	4.739E + 07
PUSfFAC -2	5.0% NaCl	−180.72	9.80E-06	148.57	143.28	1.114E-04	3.236E + 06
PUSfFAC -3	5.0% NaCl	−112.68	5.636E-06	136.92	137.28	6.532E-05	5.289E + 06
MS	Tap water	−719.55	1.155E-02	63.71	129.18	3.339E-01	160.600
PUSfFA	Tap water	−500.46	2.583E-04	123.07	145.74	2.994E-04	11.23E + 04
PUSfFAC -1	Tap water	−474.12	1.086E-05	154.46	170.23	1.258E-04	4.280E + 04
PUSfFAC -2	Tap water	−68.06	6.167E-06	96.44	98.98	7.147E-06	3.444E + 07
PUSfFAC -3	Tap water	−10.12	9.898E-08	105.57	135.15	4.516E-05	2.604E + 08

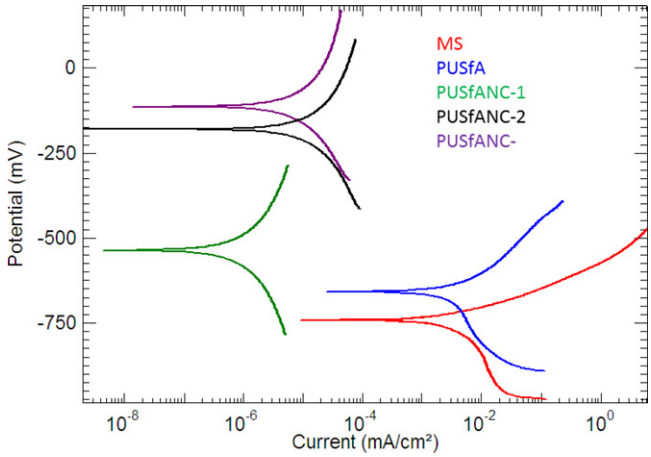

Figure 11. Tafel plot of bare MS, PUSfFA, PUSfFANC-2, PUSfFANC-2 and PUSfFANC-3 in NaCl solution.

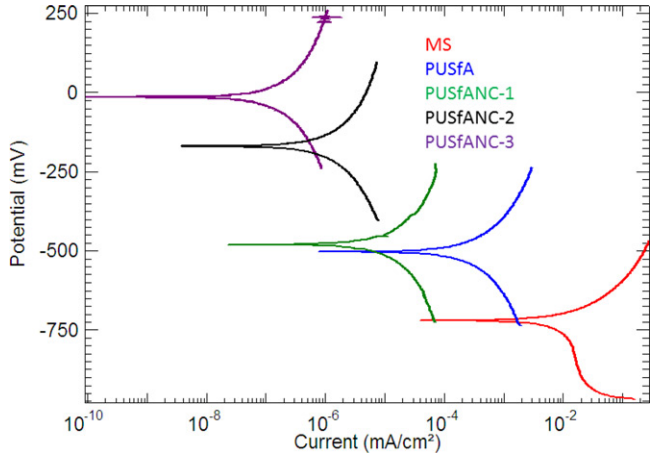

Figure 12. Tafel plot of bare MS, PUSfFA, PUSfFANC-2, PUSfFANC-2 and PUSfFANC-3 in tap water.

adhesion by strong electrostatic interaction) along with uniform dispersion of nanoTiO2 particles (fill the voids and cavities of the polymeric matrix) in nanocomposite collectively help in the formation of compact, well-adhered and crosslinked structure on metal substrate that impedes the penetration of corrosive ions via to the metal substrate, and provides protection to the metal surface from the corrosive environment (Scheme 1b). In addition to this the presence of nanoTiO2 nanoparticles in organic polymer matrix act as a strong barrier and provide a torturous path to the corrosive ions that cause a delay in the corrosion initiation and resulted in the lower Icorr and higher Rp values of nanocomposite coated CS as compared to uncoated CS.

There is well known reaction that causes corrosion in acidic medium produces Fe^{2+} ions (anodic reaction: $Fe \rightarrow Fe^{2+} + 2e^{-}$) and evolution of hydrogen (cathodic reaction: $2H^{+} + 2e^{-} \rightarrow H_2$). The nitrogen atom of the urethane linkages of the polymers get protonated in acidic medium that adsorbed on the cathode lead to mask the evolution of H_2 gas and consequently enhanced the corrosion protection. In addition to this nanostructured morphology on the surface of coatings repel the water and corrosive ions that lead to less possibility of corrosive ions attack on the surface. This mechanism can be responsible for best anticorrosive performance of PUSfFAC in acid medium.

5. Conclusion

The sunflower oil-a renewable resource has been successfully utilized as an alternative of petroleum resources for the preparation of eco-friendly polyurethane-TiO_2 nanocomposite coatings that could combat corrosion. The synthesized nanocomposite coating were amorphous in behaviour, and produced thin, flexible, glossy, scratch resistant coatings, that were thermally stable upto 275 °C, along with improved corrosion resistance performance for mild steel. We conclude that the addition of TiO_2 nanoparticles in the polymer matrix improved the overall coating properties.

Funding

The Project was supported by King Saud University, Deanship of Scientific Research, College of Science - Research Center.

References

[1] Sharmin, E.; Zafar, F.; Akram, D.; Alam, M.; Ahmad, S. Recent Advances in Vegetable Oils Based Environment Friendly Coatings: A Review. *Ind. Crops Prod.* **2015**, *76*, 215–219.

[2] Alam, M.; Akram, D.; Sharmin, E.; Zafar, F.; Ahmad, S. Vegetable Oil Based Eco-Friendly Coating Materials: A Review Article. *Arab. J. Chem.* **2014**, *7*, 469–479.

[3] Espinosa, L. M. D.; Ronda, J. C.; Galia, M.; Cadiz, V. A New Route to Acrylate Oils: Crosslinking and Properties of Acrylate Triglycerides from High Oleic Sunflower Oil. *J. Polym. Sci. A Polym. Chem.* **2009**, *47*, 1159–1167.
[4] Singh, T.; Khan, N. U.; Shreaz, S.; Hashmi, A. A. Anticandidal Activity of Cobalt Containing Sunflower Oil-Based Polymer. *Polym. Eng. Sci.* **2013**, *53*, 2650–2658.
[5] Das, B.; Konwar, U.; Mandal, M.; Karak, N. Sunflower Oil Based Biodegradable Hyperbranched Polyurethane as a Thin Film Material. *Ind. Crops Prod.* **2013**, *44*, 396–404.
[6] Omrani, I.; Babanejad, N.; Shendi, H. K.; Nabid, M. R. Preparation and Evaluation of a Novel Sunflower Oil-Based Waterborne Polyurethane Nanoparticles for Sustained Delivery of Hydrophobic Drug. *Eur. J. Lipid Sci. Technol.* **2017**, *119*, 1600283. DOI: 10.1002/ejlt.20
[7] Shendi, H. K.; Omrani, I.; Ahmadi, A.; Farhadian, A.; Babanejad, N.; Nabid, M. R. Synthesis and Characterization of a Novel Internal Emulsifier Derived from Sunflower Oil for the Preparation of Waterborne Polyurethane and Their Application in Coatings. *Prog.Org. Coat.* **2017**, *105*, 303–309.
[8] Hardia, N.; Gupta, P.; Dwivedi, R.; Mehta, A.; Basak, J.; Saxena, S.; Dixit, R.; Prasada, R. Rigid thermosetting liquid moulding resin from sunflower oil. *Ind. J. Chem. Technol.* **2011**, *18*, 271–276.
[9] Sharmin, E.; Zafar, F. Polyurethan: An Introduction, Chapter 1 and Chapter 18, InTech, Janeza Trdlin 9, 51000 Rijeka, Croatia. **2012**.
[10] Madbouly, S. A.; Otaigbe, J. U. Recent Advances in Synthesis, Characterization and Rheological Properties of Polyurethanes and POSS/Polyurethane Nanocomposites Dispersions and Films. *Prog. Polym. Sci.* **2009**, *34*, 1283–1332.
[11] Zhang, C.; Garrison, T. F.; Madbouly, S. A.; Kessler, M. R. Recent Advances in Vegetable Oil-Based Polymers and Their Composites. *Prog. Polym. Sci.* **2017**, *71*, 91–143.
[12] Petrović, Z. S. Polyurethanes from Vegetable Oils. *Polym. Rev.* **2008**, *48*, 109–155.
[13] Hojabri, L.; Kong, X.; Narine, S. S. Novel Long Chain Unsaturated Diisocyanate from Fatty Acid: Synthesis, Characterization, and Application in Bio-Based Polyurethane. *J. Polym. Sci. A Polym. Chem.* **2010**, *48*, 3302–3310.
[14] Chaudhari, A. B.; Tatiya, P. D.; Hedaoo, R. K.; Kulkarni, R. D.; Gite, V. V. Polyurethane Prepared from Neem Oil Polyesteramides for Self-Healing Anticorrosive Coatings. *Ind. Eng. Chem. Res.* **2013**, *52*, 10189–10197.
[15] Rahman, O. U.; Ahmad, S. Soy Polyester Urethane/TiO 2 and Ce-TiO 2 Nanocomposites: Preparation, Characterization and Evaluation of Electrochemical Corrosion Resistance Performance. *RSC Adv.* **2016**, *6*, 10584–10596.
[16] Ghosal, A.; Rahman, O. U.; Ahmad, S. High-Performance Soya Polyurethane Networked Silica Hybrid Nanocomposite Coatings. *Ind. Eng. Chem. Res.* **2015**, *54*, 12770–12787.
[17] Charpentier, P.; Burgess, K.; Wang, L.; Chowdhury, R.; Lotus, A.; Moula, G. Nano-TiO2/Polyurethane Composites for Antibacterial and Self-Cleaning Coatings. *Nanotechnology* **2012**, *23*, 425606.
[18] Ahmad, S.; Zafar, F.; Sharmin, E.; Garg, N.; Kashif, M. Synthesis and Characterization of Corrosion Protective Polyurethanefattyamide/Silica Hybrid Coating Material. *Prog. Org. Coat* **2012**, *73*, 112–117.
[19] Pazokifarda, S.; Esfandehb, M.; Mirabedinia, S. M. Photocatalytic Activity of Water-Based Acrylic Coatings Containing Fluorosilane Treated TiO2 Nanoparticles *Prog. Org. Coat.* **2014**, *77*, 1325–1335.
[20] Yang, J.; Han, C. R.; Duan, J. F.; Xu, F.; Sun, R. C. In Situ Grafting Silica Nanoparticles Reinforced Nanocomposite Hydrogels. *Nanoscale* **2013**, *5*, 10858–10863.
[21] Shi, H.; Liu, F.; Yang, L.; Han, E. Characterization of Protective Performance of Epoxy Reinforced with Nanometer-Sized TiO2 and SiO2. *Prog. Org. Coat* **2008**, *62*, 359–368.
[22] Somani, K. P.; Patel, N. K.; Kansara, S. S.; Rakshit, A. K. Effect of chain length of polyethylene glycol and crosslink density (NCO/OH) on properties of castor oil based polyurethane elastomers. *Polym. Sci. Part A: Polym Chem* **2006**, *43*, 797–811.
[23] Díez-Pascual, A. M.; Díez-Vicente, A. L. Development of Linseed Oil–TiO 2 Green Nanocomposites as Antimicrobial Coatings. *J. Mater. Chem. B.* **2015**, *3*, 4458–4471.
[24] Pan, H.; Wang, X.; Xiao, S.; Yu, L.; Zhang, Z. Preparation and characterization of TiO 2 nanoparticles surface-modified by octadecyltrimethoxysilane. *Ind. J. Eng. Mater. Sci.* **2013**, *20*, 561–567.
[25] Chellappa, M.; Anjaneyulu, U.; Manivasagam, G.; Vijayalakshmi, U. Preparation and evaluation of the cytotoxic nature of TiO2 nanoparticles by direct contact method. *Int. J. Nanomed.* **2015**, *10*, 31–41.
[26] Shaik, M. R.; Alam, M.; Alandis, N. M. Development of castor oil Based Poly(Urethane-Esteramide)/TiO 2 Nanocomposites as Anticorrosive and Antimicrobial Coatings. *J. Nanomater.* **2015**, *2015*, 1. http://dx.doi.org/10.1155/2015/745217
[27] Alam, M.; Alandis, N. M. Microwave assisted synthesis of urethane modified polyesteramide coatings from Jatropha seed oil. *J. Polym. Environ* **2011**, *19*, 784–792.
[28] Yadav, S.; Zafar, F.; Hasnat, A.; Ahmad, S. Poly (Urethane Fatty Amide) Resin from Linseed Oil—a Renewable Resource. *Prog. Org. Coat.* **2009**, *64*, 27–32.
[29] Mosiewicki, M. A.; Aranguren, M. I. A Short Review on Novel Biocomposites Based on Plant Oil Precursors. *Eur. Polym. J.* **2013**, *49*, 1243–1256.